Volume 51
Number 38
14 October 2022
Pages 14361-14778

Dalton Transactions

An international journal of inorganic chemistry

rsc.li/dalton

ISSN 1477-9226

ROYAL SOCIETY OF CHEMISTRY

PAPER

Matteo Bonomo, Silvia Bordiga *et al.*

A multi-technique approach to unveil the redox behaviour and potentiality of homoleptic Cu^{I} complexes based on substituted bipyridine ligands in oxygenation reactions

Dalton Transactions

ROYAL SOCIETY OF CHEMISTRY

PAPER

View Article Online
View Journal | View Issue

Cite this: *Dalton Trans.*, 2022, **51**, 14439

A multi-technique approach to unveil the redox behaviour and potentiality of homoleptic Cu^{I} complexes based on substituted bipyridine ligands in oxygenation reactions†

Barbara Centrella,‡[a] Gabriele Deplano, ‡[a] Alessandro Damin,[a] Matteo Signorile, [a] Mariagrazia Tortora, [b,c] Claudia Barolo, [a,d] Matteo Bonomo *[a] and Silvia Bordiga *[a]

The effect of differently substituted 2,2′-bipyridine ligands (*i.e.* 6,6′-dimethyl-2,2′-bipyridine, 5,5′-dimethyl-2,2′-bipyridine, 6,6′-dimethoxy-2,2′-bipyridine and 2,2′-bipyridine) on the reversible oxidation of the resulting Cu^{I} homoleptic complexes is investigated by means of a multi-technique approach (electronic and vibrational spectroscopies, DFT, electrochemistry). Among the four tested complexes, $[Cu^{I}(6,6'\text{-dimethyl-}2,2'\text{-bipyridine})_2]$ (PF_6) shows a peculiar behavior when oxidized with an organic peroxide (*i.e. tert*-butyl hydroperoxide, *t*BuOOH). The simultaneous use of UV-Vis-NIR and Raman spectroscopy methods and cyclovoltammetry, supported by DFT based calculations, allowed identifying (i) the change in the oxidation state of the copper ion and (ii) some peculiar modification in the local structure of the metal leading to the formation of a $[Cu^{II}OH]^{+}$ species. The latter, being able to oxidize a model molecule (*i.e.* cyclohexene) and showing the restoration of the original Cu^{I} complex and the formation of cyclohexanone, confirms the potential of these simple homoleptic Cu^{I} complexes as model catalysts for partial oxygenation reactions.

Received 20th April 2022,
Accepted 19th July 2022

DOI: 10.1039/d2dt01234k

rsc.li/dalton

Introduction

Copper is one of the most available transition metals in the Earth's crust and seawater;[1,2] it is usually produced in a relatively high quantity (19.7 Mtons in 2017) and low cost (6$ per kg).[3] Moreover, Cu requires lower energy for its production compared to other metals (cradle-to-gate LCA),[4] and a straightforward recycling could further decrease the CO_2-eq. emissions for its life cycle.[5] Copper is a redox active metal that, beside the metallic state (Cu^{0}), can reach three different oxidation states (Cu^{I}, Cu^{II} and Cu^{III}). Nature, as well as and synthetic and industrial chemistry, takes advantage of its one-electron (Cu^{I} to Cu^{II}) or two-electron (Cu^{I} to Cu^{III}) redox chemistry to carry out a plethora of chemical reactions, from oxygenation to hydroxylation and from C–C to C–N bond formation.[6]

To be effectively exploited as a redox catalyst, Cu^{n} needs to be stabilized by molecular ligands[7] or supramolecular structures (*e.g.* zeolites or metal organic frameworks[8–10]) preferring the former for homogeneous and the latter for heterogeneous reactions. Focusing on homogeneous complexes, an almost infinite library of ligands able to form stable complexes with both Cu^{I} and Cu^{II} centres have been designed and synthesized.[11] Among them, a central role has been played by 2,2′-bipyridine (bpy), mainly due to its low cost and synthetic easiness; indeed, bpy has been described as "the most widely used ligand"[12] in both homoleptic and heteroleptic fashions. The bpy ligands show excellent behaviour to firmly complex both Cu^{I} and Cu^{II}, enabling, when appropriately substituted, the reversibility of the oxidation state of the metal. As a matter of fact, the redox potential of the Cu^{I}/Cu^{II} couple, and thus the reversibility of the conversion, is affected by the steric hindrance nearby the metal centre.[13,14] Besides the energy required for the electron transfer, one should also consider the reorganization energy required for the conformational change, as tetra-coordinated Cu^{I} is stabilized in a tetrahedral symmetry, while Cu^{II} prefers a square planar one.[15] The energy required for the conformational change is usually relatively

[a]*Department of Chemistry and NIS Interdepartmental Center and INSTM reference center, University of Turin, via Pietro Giuria 7, I-10125 Turin, Italy. E-mail: matteo.bonomo@unito.it, silvia.bordiga@unito.it*
[b]*AREA SCIENCE PARK, Padriciano, 99, 34149 Trieste, Italy*
[c]*Elettra-Sincrotrone Trieste, S.S. 114 km 163.5, Basovizza, 34149 Trieste, Italy*
[d]*ICxT Interdepartmental Centre, Università degli Studi di Torino, Lungo Dora Siena 100, 10153 Torino, Italy*

†Electronic supplementary information (ESI) available. See DOI: https://doi.org/10.1039/d2dt01234k

‡These two authors equally contributed to the paper.

high, but it could be lowered by modulating the steric hindrance around the metal centre.[16] With opportune hindrance constraints the Cu^{I} complex can be forced toward a distorted tetrahedral geometry that can easily switch to a Cu^{II} square planar one.[17] At the same time, the square planar geometry of Cu^{II} will be distorted as well,[18] facilitating the back-reduction to the Cu^{I} state.[19] These features allowed the successful exploitation of $Cu(bpy)_{1/2}$ complexes in different fields dealing with the redox process, such as Dye-Sensitized Solar Cells (DSSCs)[20–25] and Light-emitting Electrochemical Cells (LECs)[26,27] and also as asymmetric catalysts[28] and as linkers in MOFs.[29]

Cu^{I} systems (constructed *in situ* using a Cu-salt as the copper source and bpy as the ligand, in a 1 : 1 stoichiometric ratio) in oxidation reactions of organic compounds have been extensively studied, among the others, by Stahl and coworkers.[30–33] In 2011,[30] they reported the oxidation of primary alcohols using a mixture of $Cu^{I}(ACN)_4$ as the copper source, bpy (1 eq.) and NMI (*N*-methylimidazole, 2 eq.) as ligands, molecular oxygen as the oxidant and a nitroxyl source (*i.e.* TEMPO) as the co-catalyst to regenerate Cu^{I}, thereby increasing the low catalytic efficiency previously reported.[34] They proved that this Cu^{I} mixture leads to an almost quantitative yield only if the Cu source is a Br^{-} salt, whereas very poor yields are obtained in the presence of Cl^{-} salts. A couple of years later, Stahl[31] successfully tested similar mixtures for the oxidation of secondary alcohols (with ABNO as the nitroxyl radical): the decoration of the bpy ligand with methoxyl groups at the 4-4′ position provided a higher yield, whereas no oxidation was detected using 6,6′-dimethylbipyridine. The same group also investigated the oxidation of amines to imines[32] and the lactonization of diols[33] using analogous systems. They tested different substituents at the 4,4′ position (*i.e.* methyl, methoxyl or tertbutyl) showing comparable yields; indeed, replacing NMI with DMAP (in a 2 : 1 ratio with respect to the Cu source) further improves the reaction yield, especially in coordinating solvents (*e.g.* THF, DMSO...). A similar approach (a mixture of CuBr : 6,6′-^{t}Bubpy : DMAP 1 : 1 : 3 in ACN) has also been reported by Oisaki and Kanai,[35] for the oxidation of amines to imines and C–C couplings: in this case, ^{t}Bu-substituted bpy outperforms bpy. Chiba reported the incorporation of atmospheric oxygen in activated *N*-alkylamidines leading to the oxidation of a tertiary C–H bond:[36] in this case, phen-based mixtures lead to better yields than bpy-based systems.

It should be recalled that bpy-based Cu^{II} supramolecular systems (*i.e.* MOFs[37,38]) as well as other $Cu^{I/II}$ mixtures[39–42] based on N-chelating ligands (in a 1 : 1 ratio) have been exploited in oxidation, oxygenation or hydroxylation reactions, but their discussion falls outside the aim of the present paper. On the other hand, the literature on Cu : bpy 1 : 2 mixtures for oxygenation reactions is extremely scarce. To the best of our knowledge, the only report on Cu^{I} systems by Sawyer dates back to 1993:[43] the bpy ligand was mixed in a 2 : 1 ratio with a Cu^{I} source in the ACN/pyridine system using H_2O_2 or *t*BuOOH as the oxidant; cyclohexane or cyclohexene was oxidized to the corresponding peroxides and ketones with a relatively low yield (that is three times higher for the unsaturated substrate). They proposed (but not validated) different reaction patterns initiated by the deprotonation of the peroxide reactant mediated by pyridine that leads to the formation of a reactive Cu–OOR intermediate. Similarly, Repo *et al.*[44] reported the use of a Cu^{II} : bpy 1 : 2 mixture for the oxidation of 2,2′-biphenol proving that the substitution of the bipyridine ligand is of pivotal importance in the tuning of the catalytic activity.

In all the described approaches, the main proposed reaction mechanism involves the formation of hydroperoxide species bound to the metallic center, as also proved by the production of ROOH (where R is an aliphatic substrate) as the main product.[41] However, $Cu(bpy)_{1/2}(L)_{0/2}$ complexes are always obtained *in situ* by mixing a stoichiometric amount of the ligand and Cu source in ACN. Although this methodology leads to the product formation and avoids an additional synthetic step, it has a major drawback: as brilliantly evidenced by Tuczek,[45] the one-pot approach does not allow controlling the real chemical structure of the catalyst; as a matter of fact, apart from the desired (or proposed) one, other species (involving both homoleptic systems and heteroleptic ones and also including the solvent as the possible ligand[46,47]) are likely to form. Indeed, ACN has a recognized coordination power[48] and could induce ligand exchange (especially if present in a very large excess, as occurring when it is adopted as a solvent); this equilibrium is further complicated if pyridine (as a base) is added,[49] due to its even higher coordination ability. To avoid this issue, two approaches could be followed: (i) the *ex situ* synthesis (and characterization) of the complexes to be used as catalysts and/or (ii) the development of an accessible experimental method to follow the chemical modification of the complexes during the reaction. A first step toward (i) has been recently made by Shul'pin *et al.* synthesizing both Cu^{I} and Cu^{II} phenanthroline-based homoleptic complexes (possibly modified with an additional ancillary ligand) having a fair activity (in the Cu^{II} form) for the oxidation of cyclohexene by H_2O_2 in ACN. Nevertheless, it should be pointed out that, even in this case, the integrity of the complexes after the dissolution in ACN has not been proved.

Throughout this paper, we select and synthesize four different homoleptic $Cu^{I}(bpy)_2$ complexes aiming at investigating the effect of the nature and position of the substituent of 2,2′-bipyridine on the redox behaviour of the Cu center. A multi-technique approach (electronic and vibrational spectroscopies and electrochemistry) supported by computational analyses is exploited to investigate the chemical modification of Cu complexes undergoing a redox cycle by exploiting a combination of different solvents and oxidants. We highlight that the 6,6′-dimethyl-2,2′-bipyridyl Cu^{I} complex shows a peculiar reversibility, strongly differing from its homologues. Thus, a more detailed dynamic analysis (simultaneous time-resolved UV-Vis-NIR and Raman analyses) of this system, conducted at Elettra synchrotron, proved almost quantitative reversibility of the redox cycle and the ability to easily oxidize a targeted molecule (*i.e.* cyclohexene).

Results and discussion

Design of modified 2-2′-bipyridine ligands and selection of oxidation conditions

Among the various modifiers to decorate the 2-2′-bipyridine skeleton, methyl was selected as the simplest substituent bound both at the 6,6′ and 5,5′ positions leading to 6,6′-dimethyl-2,2′-bipyridine (coded BPA) and 5,5′-dimethyl-2,2′-bipyridine (BPB), respectively; as a modifier impacting both the electronic properties and the steric hindrance of the ligand, methyl was replaced by a methoxy moiety (6,6′-dimethoxy-2,2′-bipyridine, BPC). To have a comparison with literature data,[43] the unsubstituted 2,2′-bipyridine (BPD) was also considered. To obtain the complexes, the ligands were reacted with tetrakis(acetonitrile)Cu(I) hexafluorophosphate as both a copper and counterion source (see Scheme 1 and the Experimental section for further details); indeed, the ligand exchange reaction was promoted by the higher coordination strength of the bipyridine ligands: as a result, [Cu^{I}(6,6′-dimethyl-2,2′-bipyridine)$_2$] (PF_6) (CuBPA), [Cu^{I}(5,5′-dimethyl-2,2′-bipyridine)$_2$] (PF_6) (CuBPB), [Cu^{I}(6,6′-dimethoxy-2,2′-bipyridine)$_2$] (PF_6) (CuBPC) and [Cu^{I}(2,2′-bipyridine)$_2$] (PF_6) (CuBPD) were obtained with almost quantitative yields. It is noteworthy that complex formation reactions are fast and easy to reproduce, making the process inexpensive and scalable.

Aiming at driving a homogeneous redox reaction, the choice of both the solvent and oxidant (to be used in conjunction with the Cu complexes) is crucial, and it could seriously impact the effectiveness of the reaction. In this context, the most exploited solvent in the literature is ACN, that is also valuable for its (electro)chemical inertness and its well-known simple spectroscopic fingerprint, that allows one to predict the signals of the sample.[50] Unfortunately, when dissolved in ACN, all the complexes, but CuBPA, tend to degrade quickly, as proved by the loss of color of the solution (Fig. S1†). This was attributed to a ligand exchange between all of the three BPB, BPC, and BPD and ACN, ascribable to the large excess of the latter.

To further prove this instability, we dissolved Cu^{I}(bpy)$_2$ complexes in degassed ACN; even in this case, a colorless solution is obtained proving the loss of the MLCT band (*vide infra*); very interestingly, when the solvent is allowed to slowly evaporate (under nitrogen), a more and more reddish solution is obtained, and when all the solvent is removed, a dark red powered is obtained, proving that the instauration of a ligand exchange equilibrium is the main reason for instability. A partial oxidation of Cu^{I} due to atmospheric oxygen could not be completely excluded. These results match well with the evidence found in a previous paper by some of us[51] and with the results of Sawyer *et al.*[43] The kinetics of the ligand exchange reaction is sensibly influenced by the nature of the substituent and its position on the bipyridine ligand;[52] specifically, it is really fast for CuBPB and CuBPD and a bit slower for CuBPC; on the other hand, only limited reaction (tested by mass spectrometry, not shown) occurred with CuBPA, ascribable to the higher steric hindrance of the methyl moieties (at the 6,6′ position).

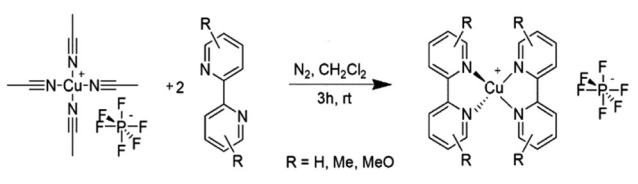

Scheme 1 Scheme of synthetic procedure.

Thus, we were forced to change the solvent, and we resolved to dichloromethane (DCM), which ensures a high solubility of Cu^{I} complexes coupled with a well-known spectroscopic fingerprint. Unfortunately, Cu^{II} counterparts are insoluble in DCM, preventing us to propose a comparison with the reduced complexes. A possible strategy to improve the solubility of [Cu^{II}(bpy)$_2$]$^{2+}$ complexes consists of the use of ancillary ligands (*i.e.* Cl^-), but this will seriously impact the complexes' geometry, making a comparison unreliable.

With respect to the oxidant, both hydrogen peroxide (H_2O_2) and *tert*-butyl hydroperoxide (*t*BuOOH) have been tested relying on the literature.[43,50,53] The former is more reactive[54] but it has a high water content, whereas the latter's reaction, a milder oxidant,[55] could be more easily controlled. Hydrogen peroxide (30% w/w in water) is just partially soluble in DCM; therefore, when the oxidation reaction occurs, the resulting Cu^{II} complex is mainly observed in water, as proved by the greenish color of the aqueous phase; only traces were found in the organic phase. Thus, we resolved to *t*BuOOH, assuring a homogeneous organic phase. The milder reactivity of *t*BuOOH could be fairly considered as a valuable point in order to finely tune the reactivity of CuPBX by the ligand design. To precisely follow the redox processes and to detect the involved species, we exploited a multi-technique approach (*i.e.* cyclic voltammetry, Raman, UV-Vis-NIR). Indeed, it will be immediately concluded that the nature of the ligands complexing Cu^{I} heavily impacts the oxidation process.

Electrochemical characterization of pristine and oxidized complexes

Cyclic voltammetry, more generally electrochemistry, is one of the techniques of election to investigate the oxidation state of metal complexes due to the high electroactivity of the metal centre.[56] This also implies that the redox potential of the complexes could be dramatically influenced by the nature of the ligands accounting for both electronic and steric effects. In the present case, the ligand could influence the accessibility of oxidant species to the copper centre. The voltammograms of the pristine and oxidized (with *t*BuOOH) complexes are reported in Fig. 1.

All the complexes show good electrochemical stability in DCM (no changes are highlighted upon continuous cycling), and the voltammograms are characterized by a reversible redox peak, the position of which strongly depends on the

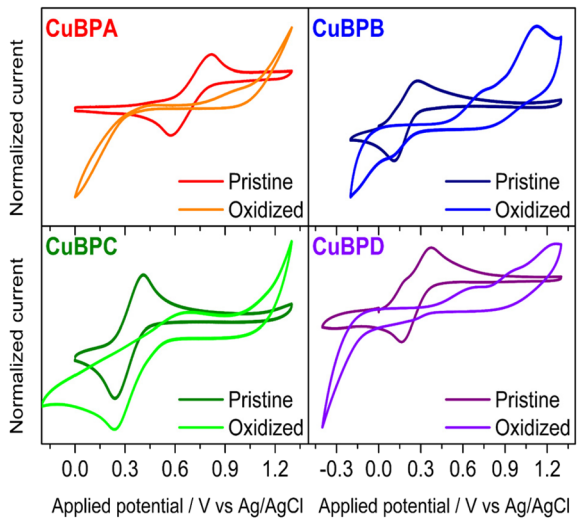

Fig. 1 Cyclovoltammograms of pristine complexes (darker lines) and after 50 cycles from the addition of *t*BuOOH (0.1 ml of *t*BuOOH 5.5 M *n*-decane solution) as oxidant (lighter lines). Complexes were dissolved (5 mM) in a solution of DCM containing $TBAPF_6$ (0.1 M) as a supporting electrolyte. CV's starting potential has been set to 0 V *vs.* Ag/AgCl and the scan is conducted toward positive values.

nature of the ligand. $E_{1/2}$ of the unsubstituted bipyridyl complex (CuBPD) is located at 269 mV *vs.* Ag/AgCl; the insertion of methyl in position 5 (CuBPB) just slightly influences the electrochemical behaviour of the complex leading to a more easily oxidizable copper atom ($E_{1/2}$ = 190 mV). The insertion of methoxy moieties in the ligands at positions 6 and 6′ (CuBPC) leads to a less easily oxidizable system ($E_{1/2}$ = 324 mV); this could be due to a higher hindrance of the methoxy group. Recently, Giordano *et al.*[51] pointed out that the oxygen could partially coordinate the copper atom reducing its proneness to oxidation. According to the literature,[57] CuBPA shows the highest redox potential ($E_{1/2}$ = 697 mV) due to the steric hindrance of the methyl group that likely causes more severe distortion of the oxidized complex geometry (see τ parameter in Table S1†). This trend is in good agreement with the one calculated using DFT (Table S1†). Indeed, the higher potential of CuBPA could also be an indicator of a more energetic-costly $Cu^{I} \rightarrow Cu^{II}$ transition. CVs could also give some insights into the $Cu^{I} \rightarrow Cu^{II}$ redox kinetics, with ΔE_p (*i.e.* the voltage difference between the oxidation and reduction peaks) being directly related to the latter;[58] the higher ΔE_p, the lower the kinetic of the electronic oxidation. Within the analysed complexes, CuBPA shows a higher ΔE_p (0.24 V) followed by CuBPD (0.21 V), CuBPC (0.17 V) and CuBPB (0.16 V), that are comparable to that of the Fc/Fc^+ couple (0.27 V).

The effect of substituents is even clearer after the addition of the oxidant (*t*BuOOH): as soon as the latter was added, the voltammograms evolved differently as a consequence of the substitution on the pyridine rings. No matter the complex involved, the electrochemical oxidation is always faster compared to the simple addition of an oxidant. This proves that the oxidation is (partially) assisted by potential cycling. After 50 cycles from the addition of *t*BuOOH, the voltammogram of CuPBA is almost flat, proving that the concentration of the reduced form of the complex is close to zero, as also evidenced by UV-Vis-NIR (*vide infra*). A small shoulder could still be detected at *ca.* 1 V, which could be ascribed to the presence of *meta*-stable species generated throughout the oxidation process: indeed, this shoulder tends to vanish at longer times. As expected, CuBPB and CuBPD behave similarly; the voltammograms of both the complexes are completely flat in the oxidation scan up to 0.6 V, but they present a more pronounced shoulder at 740 mV and 640 mV, respectively. Very interestingly, an irreversible oxidation process could be evidenced at a potential higher than 0.9 V, which could be likely ascribed to the oxidation of the ligand.

This process seems to be catalyzed by the presence of a metal; as a matter of fact, the sole ligands (Fig. S2†) do not show any oxidation process at $V < 1.2$ V even after the addition of *t*BuOOH. Another interesting point could be evidenced: while CuBPA's voltammogram is almost flat throughout the reduction cycle, CuBPD and (even more) CuBPB show an irreversible, very broad reduction peak; the latter is placed at the same potential of the $Cu^{II} \rightarrow Cu^{I}$ reduction, well correlating with literature reports.[43] This is a fair hint that the addition of *t*BuOOH leads (at least partially) to pure electronic oxidation, the result of which is a Cu^{II} complex that does not involve the presence of any oxo-species. This feature is even more evident when CuBPC is oxidized, for which a sharp and irreversible peak (0.27 V *vs.* Ag/AgCl) is recorded. The absence of an associated oxidation peak is due to the presence of *t*BuOOH (added in excess) in the solution that chemically re-oxidizes the Cu^{I} complex as soon as the latter is electrochemically produced.

Characterization of electronic transitions of the pristine and oxidized complexes

Before going into detail with the description of the effect of the oxidation/oxygenation process on different complexes, a precise assignment of the electronic transitions observed experimentally has been conducted supported by DFT. Indeed, the simulated results are in good and qualitative agreement with the experimental ones (Fig. S3–S5† and related discussion), thus making them valuable support for the interpretation of the data-set presented hereafter. The UV-Vis spectra of the four Cu complexes, both in their pristine state and in two different oxidation pathways (*i.e.* using $NOPF_6$ or *t*BuOOH), are reported in Fig. 2 (top frame). The choice of *t*BuOOH was discussed above, whereas $NOPF_6$ was also tested as an alternative oxidizing agent because of the suspicion of oxygenated species formed. It is reported in the literature that the NO^+ species is able to oxidize metal centres with a single electron transfer mechanism, releasing gaseous NO.[19,22] However, due to the good coordination ability of nitrosyl molecules,[59,60] the formation of a Cu^{II}–pentacoordinate species could not be *a priori* excluded. Therefore, *t*BuOOH could likely lead to the formation of a Cu^{II}–$O(bpy)_2^+$/Cu^{II}–$OH(bpy)_2^+(PF_6^-)$ species, whereas $NOPF_6$ would preferably form $Cu^{II}(PF_6)_2$ with likely a

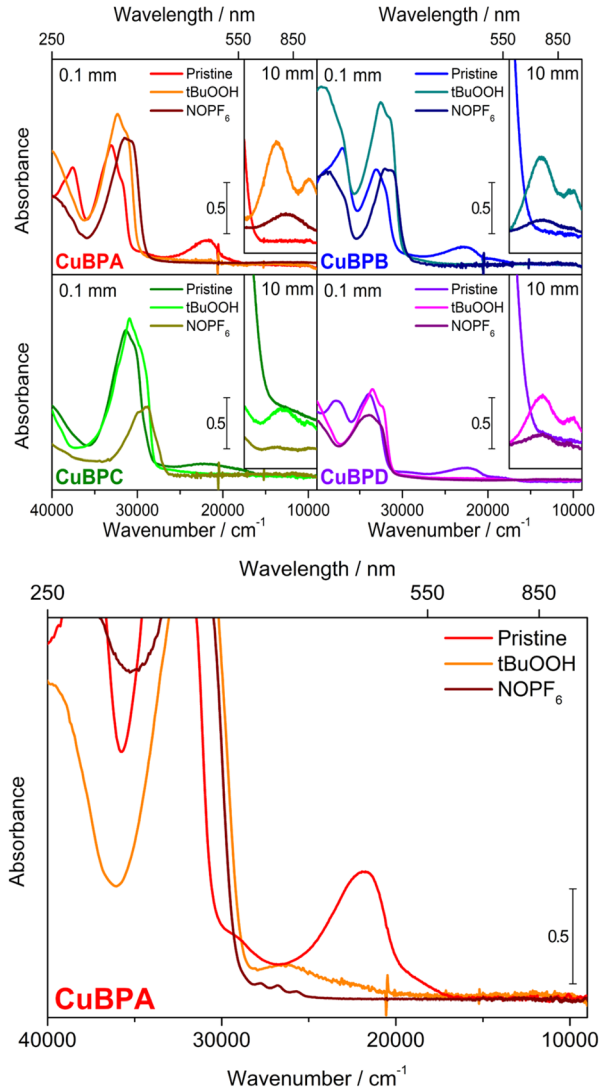

Fig. 2 Top: UV-Vis spectra of the four complexes in their pristine form and after reaction with *t*BuOOH and $NOPF_6$. Solutions were prepared with a concentration of 5 mM (DCM). Data in the inset show the spectra in the region 17 500–9000 cm^{-1}, in correspondence with the *x*-scale in the main panels. Main panel: 1 mm optical path. Inset: 10 mm optical path. The spectra for the two cuvette thicknesses were registered simultaneously on the same sample solution recirculating between the two and a reservoir. Spectra are reported in absorbance without any additional treatment. Bottom: Zoom of UV-Vis to highlight the occurrence of the band at 26 500 cm^{-1} (377 nm) after the oxidation with *t*BuOOH. Optical path: 1 mm.

NO ancillary ligand. By comparing the final state of the complexes that reacted with the two oxidants, one could discriminate electronic oxidation from oxygenation since the two possible outcomes should present different electronic structures and geometries.

In their pristine form, the complexes show two main peaks located around 28 000 cm^{-1} and 22 000 cm^{-1} (Fig. S3†). On the basis of a natural transition orbital (NTO, see Fig. S6† for Cu^{I}BPA) analysis of the simulated electronic transitions, this peculiar band is ascribed to a metal to ligand charge transfer (MLCT) from the Cu d_{xz} orbital (hybridized with some N sp^2 orbitals) to the π^* orbitals of the ligands.[61] The differences between the complexes in the region above 28 000 cm^{-1} are mainly due to the differences in the structure of the ligands (Fig. S7†). The high energy contribution, represented by the simulated transition at 35 000 cm^{-1}, is instead due to a second MLCT from the Cu d_{z^2} orbital to the π^* orbitals of the ligands. The identified MLCT is of particular interest since they can be exploited to achieve resonant Raman conditions with opportune excitation wavelengths, thus allowing a preferential enhancement of vibrational modes having the same symmetry as that for the electronic transition (thus strictly related to the Cu^n cation). One should note that this evidence is not consistent with the UV-Vis spectra of CuBPD (obtained *in situ* in ACN) reported by Sawyer *et al.*;[43] they showed a spectrum without any transition in the visible region. This observation could suggest that the effective formation of a $Cu^{I}(bpy)_2^+$ complex is not occurring under these conditions.

Meaningful changes appear in this region for all complexes upon oxidation: they arise from a combination of structural and electronic effects, as they result from both perturbation of the ligand transitions and differences in the MLCT transitions. On the other hand, the band around 22 000 cm^{-1} differs slightly between the complexes, but disappears completely for all of them upon oxidation, with a subsequent appearance of one or two bands in the region between 17 500 and 9000 cm^{-1} (Fig. 2, top frame insets); the latter is assigned to d–d transitions on the metal centre. Interestingly, most complexes show two distinct bands at around 13 700 and 10 000 cm^{-1}, likely indicating a geometrical distortion of the d^9 system; the only exception in this trend is that CuBPA is oxidized using $NOPF_6$, suggesting differences in the coordination structure of this sample for the two oxidation pathways.

As can be seen in Fig. 2 (bottom frame), CuBPA is also characterized by a peculiar absorption at 26 500 cm^{-1} (377 nm) after oxidation with *t*BuOOH (absent when treated with $NOPF_6$); the intensity of this peak is five times more intense than the main d–d transition. This band could be fairly attributed to the formation of an oxygenated species (*i.e.* Cu^{II}–$O(bpy)_2^+$, Cu^{II}–$OH(bpy)_2^+$ or Cu^{II}–$OOH(bpy)_2^+$, *vide infra*) and it accounts for the different coloration of the *t*BuOOH-oxidized solutions (see Fig. S8†). On the other hand, the spectra of the other samples seem to be very similar, no matter the nature of the oxidant; this could be fairly ascribed to the lower protection offered by the ligands other than BPA. Interestingly, a sizeable drop in the intensity of the d-d transition is observed upon oxidation with $NOPF_6$: this is most probably due to solubility issues (bare Cu^{2+} complexes are less soluble in DCM than Cu^+ ones), also causing precipitation (*i.e.* a blue precipitate could be detected) and the formation of suspensions, decreasing the collected signal as a consequence of scattering phenomena.

Characterization of vibrational modes of the pristine and oxidized complexes

The reaction of Cu complexes in DCM solutions with the *t*BuOOH oxidizing agent has also been followed by Raman

Spectroscopy, adopting the experimental set-up described in the Experimental section and choosing a 244 nm exciting laser line to fully exploit the resonance conditions, thus overcoming possible scarce sensitivity due to the adopted concentration. It is worth mentioning here that DFT calculations are able to properly reproduce the position of the peaks in the Raman spectra of the parent solid powders thus making them valuable support for the interpretation of the data-set presented hereafter. A more detailed analysis is provided in the SI (Fig. S9–S11† and related discussion).

The results are reported in Fig. 3, where the spectra obtained for the pristine/oxidized complexes (solid colored lines) are compared with those obtained for the respective parent ligands (solid grey lines) and bare DCM (solid black line). For the sake of comparison, the Raman spectra obtained for the pristine/oxidized complexes are normalized at the DCM peak falling at 1425 cm^{-1}. As it can be seen from the reported data, the reaction with *t*BuOOH causes just small variations in the Raman spectra of the complexes when compared to those obtained for the pristine ones; this suggests that the original structure of the Cu containing complexes is maintained after the reaction (also testified by the fact that no clear bands ascribable to bare ligands appear after *t*BuOOH addition), further highlighting the peculiarity of our approach.

However, a closer inspection of the spectra of the CuBPA (see also Fig. S12†) and CuBPD complexes reveals a blue-shift ($\Delta\nu_1$ = +10 cm^{-1} for both complexes, and +20 cm^{-1} with respect to the bare ligands in the *trans* configuration) of the peaks at 1014 cm^{-1} and 1028 cm^{-1} (ν_1^{Cu}), respectively, after interaction with *t*BuOOH; this shift is very faint in CuBPC and not observable for CuBPB. Furthermore, with respect to the CuBPA complex, a blue-shift of the peak at 1324 cm^{-1} (ν_2^{Cu}) can be observed ($\Delta\nu_2$ ~+10 cm^{-1}). From the reported data, it can be concluded that Raman Spectroscopy can be fruitfully used to follow the reactivity of such complexes with respect to oxidizing agents.

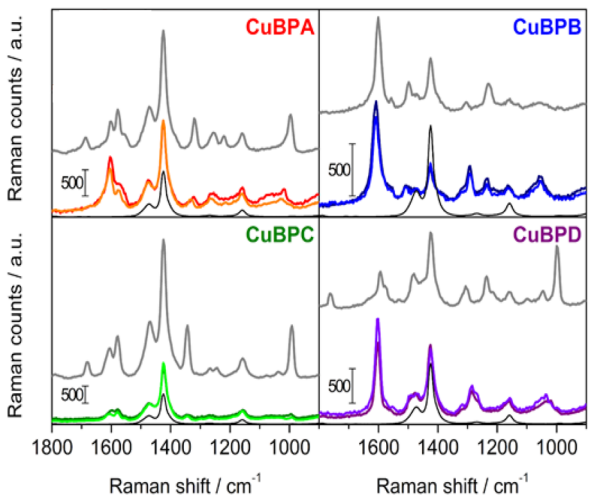

Fig. 3 Raman spectra of DCM solutions of ligands (grey curves), pristine complex and oxidized complexes for CuBPA (red panel), CuBPB (blue panel), CuBPC (green panel), CuBPD (violet panel). In all the panels, darker colour refers to the solution after the addition of *t*BuOOH. DCM spectrum (in black) is reported for the sake of clarity (black curves).

Evidence from the proposed multi-technique approach

The proposed multi-technique approach allows us to highlight a dramatic influence of the nature and the position of a substituent on the oxidation (oxygenation) reaction of 2-2′-bipyridine-based Cu^{I} complexes. As a matter of fact, each technique provides interesting but sometimes partial insights. UV-Vis-NIR spectroscopy shows, after the addition of an appropriate oxidant, the formation of a Cu^{II} species as proved by the occurrence of d–d transitions at higher wavelengths (the inset in the top frame of Fig. 2). Indeed, for CuBPA, the choice of the oxidizing agent seems to be particularly meaningful, leading to different spectra when $NOPF_6$ is employed in place of *t*BuOOH. Indeed, the peculiar behaviour of CuBPA could be clearly evidenced by the presence of an additional peak at 26 500 cm^{-1} (CuBPA treated with *t*BuOOH). This unique behavior of CuBPA could be rationalized by referring to the electrochemical data of all the complexes: CuBPA shows remarkably higher redox potential and, once oxidized, it becomes electrochemically inactive in the investigated potential window; this is a fair evidence that, on the one hand, Cu^{II}BPA is not the (main) result of the oxidation and, on the other hand, the product of the oxidation is stable and does not immediately react with other species or incur in self-oxidation reactions. The other complexes seem to have a different fate as a results of the addition of *t*BuOOH; CuBPC tends to be oxidized to its initial Cu^{2+} form as proved by the persistence of the electrochemical reduction peak at 0.27 V and Cu^{II}BPC is particularly stable due to the effect of the methoxy groups close to the copper site. CuBPB and CuBPD, instead, seem to incur in a (partial) self-oxidation reaction as proved by the appearance of an additional oxidation peak at $V > 0.5$ V.[43] In this context, Raman analyses are very meaningful to highlight that the reaction with *t*BuOOH does not significantly impact the vibrational transitions characteristic of each system, proving that the oxidation process neither dramatically changes the chemical environment of the metal centre nor destroys the ligand.

The findings mentioned above prove that CuBPA shows a peculiar behaviour, likely giving rise to stable oxygenated $Cu^{II}(bpy)_2^{+}$ species. To further investigate the nature of such species, we performed DFT simulation of the UV-Vis and Raman spectra for some hypothetical structures (whose optimized geometries are reported in Fig. S13†). The outcomes, compared with experimental results, are reported in Fig. 4. By qualitative comparison of the experimental UV-vis spectrum of CuBPA oxidized by *t*BuOOH with the simulated spectra of Cu^{II}–$O(bpy)_2^{+}$ and Cu^{II}–$OH(bpy)_2^{+}$, both the models show electronic transitions in the 25 000–30 000 cm^{-1} region.

In detail, the CuBPA–OH structure better reproduces the experimental profile, with a well-distinguished band peaking at 29 000 cm^{-1}. This assignment is further confirmed by the good agreement of the calculated d–d transitions for Cu^{II}–OH

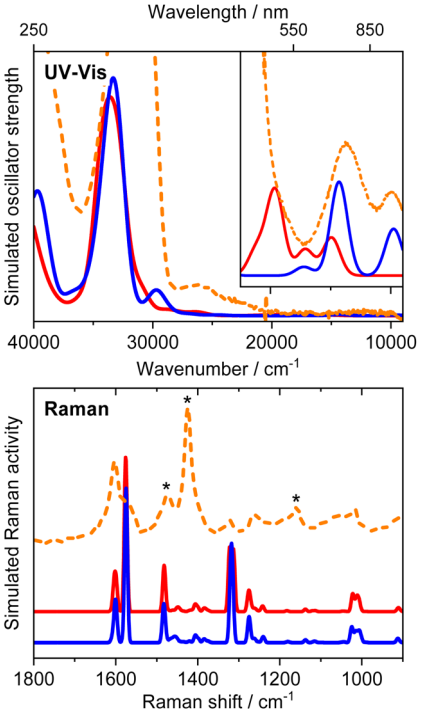

Fig. 4 Computed (solid lines) UV-Vis (top frame) and Raman (bottom frame) spectra *vs.* experimental ones (dashed lines) for CuBPA bearing a Cu–O_x specie: oxyl- (red lines) and hydroxo- (blue lines). Experimental UV-Vis has been collected with an optical path of 1 mm. Experimental Raman has been collected with a 244 nm excitation wavelength (asterisks highlight the features of DCM). Simulated spectra have been convoluted with Gaussian functions (FWMH set to 5 cm^{-1} for Raman, to 1000 cm^{-1} for UV-Vis). Computed vibrational frequencies have been scaled by a multiplicative factor (0.978).

$(bpy)_2^+$with those experimentally observed. Other options, such as Cu^{II}–$OOH(bpy)_2^+$ or $Cu^{II}(bpy)_2^+$ (Fig. S14†) seem to be unlikely, showing simulated spectra that sizeably differ from the experimental ones (especially when electronic transitions are considered). One should note that the selected functional and basic set are in line with the ones conventionally exploited in the literature (Table S2†).

This assignment is also supported by the thermodynamic stability of the species, as the Gibbs free energy of formation (calculated according to the reactions shown in Scheme S1†) for Cu^{II}–$OH(bpy)_2^+$ is lower than that of Cu^{II}–$O(bpy)_2^+$ or Cu^{II}–$OOH(bpy)_2^+$ (26.9 kJ mol^{-1} *vs.* 36.3 kJ mol^{-1} or 214.8 kJ mol^{-1}, respectively). In the case of Raman spectroscopy, unfortunately, specific Cu–O modes are not detectable under the adopted experimental conditions. Nonetheless, the simulated spectra for Cu^{II}–$O(bpy)_2^+$, Cu^{II}–$OOH(bpy)_2^+$ and Cu^{II}–$OH(bpy)_2^+$ show a shift for the ν_1^{Cu} mode observed between +25 and +32 cm^{-1} with respect to *trans*-BPA, in line with experimental results. This result confirms that the models correctly account for the screening effect of the O/OH group on the Cu^{II} ion, as the $\Delta\nu_1^{Cu}$ value obtained for a isolated Cu^{II} is +38 cm^{-1} from simulation (Table S3†). A further confirmation could be obtained from the quite good correlation between q/r (the elementary charge/ionic radius ratio of M^{m+}) and computed $\Delta\nu_1$ between pristine *trans*-BPA and *cis*-BPA in the M^+ complex (Fig. S15†) for the calculation performed on M^{m+}(*cis*-BPA)$_2$ (where M^{m+} = Li^+, Na^+, K^+, Cu^+, Be^{2+}, Mg^{2+} or Ca^{2+}); indeed, $\Delta\nu_1^{Mm+} > 0$ has been observed for the BPD interacting with the surface species of SiO_2 and Al_2O_3.[62]

Aiming at proving the reversibility of the oxygenation reaction experimented by the Cu site, we treated the oxidized solution with a common oxidizable substrate (*i.e.* cyclohexene); after the addition, the solution of oxidized CuBPA turns to a dark orange solution (*i.e.* the same as pristine CuBPA, *vide infra*). This reversibility is even more clear when the reaction between activated CuBPA and cyclohexene is followed by CV (Fig. S16†): indeed, after the addition, the voltammogram evolves towards the characteristic redox peaks of Cu^IBPA. Complementary findings have been obtained by coupling Raman (@Elettra synchrotron) and UV-Vis spectroscopy with an *in situ* approach (*vide infra*). However, other complexes, namely CuBPB, CuBPC and CuBPD, do not show the same behaviour: indeed, no remarkable modifications could be evidenced after the addition of cyclohexene, proving that the oxygenated species, if obtained and stable, are not reactive enough (or not able) to promote the oxidation of cyclohexene.

Exploitation of the *in situ* synchrotron-based Raman/UV-Vis simultaneous set-up

As proved in the previous section, CuBPA shows a peculiar behaviour compared to the other complexes tested within this work. Electrochemistry proved that once oxidized, CuBPA is able to return to its Cu^I state when an appropriate reductant is added. This observation is supported by the fact that the most probable species, *i.e.* Cu^{II}–$OH(bpy)_2^+$, has a slightly positive formation energy (*i.e.* 23.3 kJ mol^{-1}), and thus the hydroxyl moiety is potentially reactive toward a reductant. It should be noted that electrochemistry gives meaningful insights into the electroactive species only and, thus, eventual degradation of the complexes or the formation of products of interest could be hardly detectable. Moreover, the continuous supply of electrons (due to the CV approach) could have no trivial effect on reduction reaction catalysis.

To further shed light on the reactivity of the selected complex during its redox cycle, we resolved to joint and simultaneous monitoring of the reaction solution by means of both vibrational and electronic spectroscopy. This allows us to finely detect some modification of the different substrates in the reaction solution. Following this idea, it clearly appears that the adopted exciting laser line (*i.e.* 244 nm) can suffer from sensitivity problems (Fig. 3, red panel): in fact, ν_1^{Cu}, even if still visible, undergoes a drastic loss in intensity after CuBPA reacts with *t*BuOOH. This is mainly ascribable to a change in energy for reaching resonance conditions in the reacted system, limiting our ability to finely follow the redox cycle. To avoid this, at the synchrotron facility Elettra, we finely screened the excitation wavelengths (*i.e.* 226 nm, 244 nm and 266 nm) and by selecting the 266 nm line we were able to obtain clear spectra for all the tested solutions. The major drawback in the

employment of synchrotron radiation is the relatively low intensity of the incident radiation in the exploited range, forcing us to use relatively long acquisition times and to average the measurements on 3 scans at least. It was possible to record one Raman spectrum every 30 minutes, much slower than the time resolution ensured by the UV-Vis-NIR set-up (one spectrum each minute). The effect of oxidant (*i.e.* *t*BuOOH) and (then) reductant (*i.e.* cyclohexene) addition could be finely followed by means of UV-Vis-NIR spectroscopy (Fig. S17†); as soon as *t*BuOOH is added to a 1 mM solution of CuBPA, the intensity of the characteristic absorption peak starts to slowly but constantly decrease and simultaneously a broad peak (at 26 500 cm^{-1}) grows. After 150 minutes, the electronic spectrum of oxidized CuBPA is invariant. At this stage, the Raman spectrum of the same solution (green profile in Fig. 5) presents two main differences compared to the spectrum recorded at t = 0 (red profile in Fig. 5): a clear shift toward a lower Raman shift of the band at 1050 cm^{-1} and a broadening of the peak at 1600 cm^{-1}. The former is directly related to the change in the coordination of the metal ion, and it is consistent with the formation of a Cu^{II}–$OH(bpy)_2^+$ species (*vide supra*), whereas the latter is directly related to the vibrational modes of the bipyridine ring and, thus, less sensitive to the charge state of the metal. This could be ascribable both to a change in the geometry of the ligand and to the irreversible oxidation of the latter. To check this and to eventually prove the reversibility of the oxidation process of the Cu centre, we added an equimolar (with respect to *t*BuOOH) amount of cyclohexene. Following this addition, the UV-Vis-NIR (Raman) spectrum of the solution starts to rapidly evolve, and the recovery of the peak centred at 22 000 cm^{-1} can be easily detected. After only 90 minutes from the addition (t =

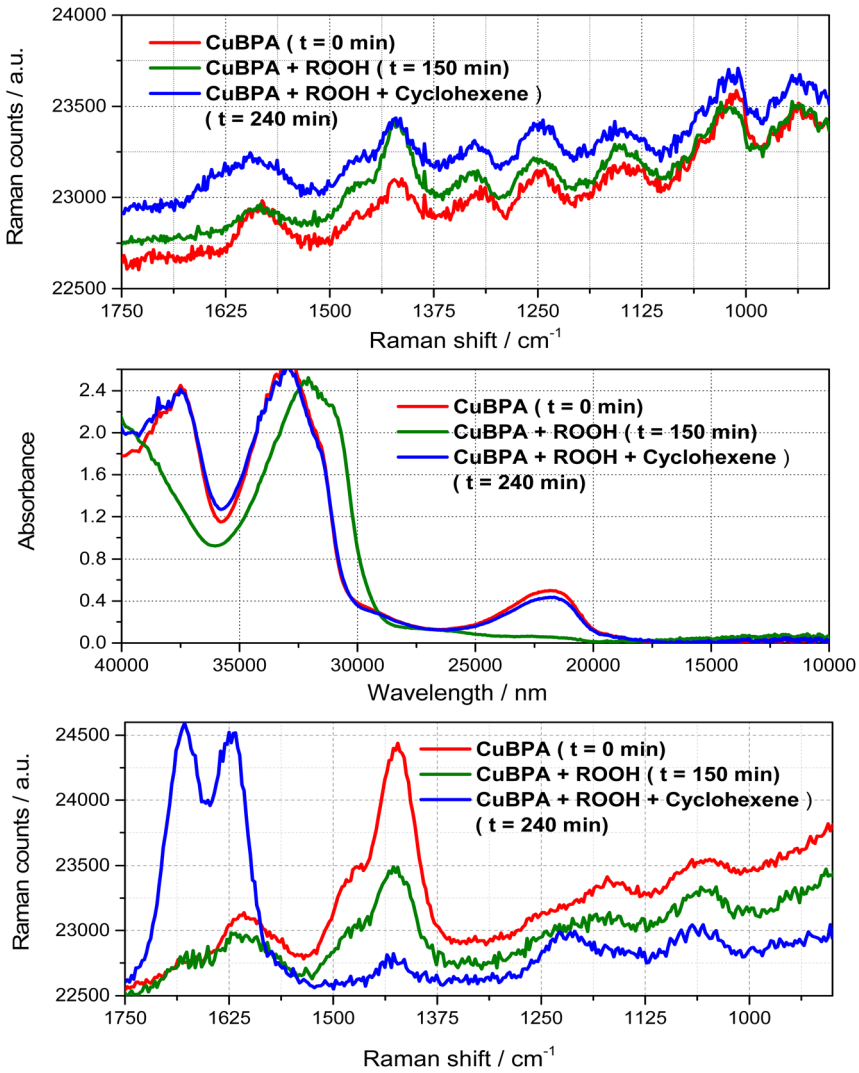

Fig. 5 Synchrotron Raman (top) and UV-Vis-NIR (middle) spectra of pristine CuBPA solution (1 mM in DCM, red lines) and after the addition of *t*BuOOH (green lines) and cyclohexene (blue lines). Measurements are made simultaneously on the same solution exploiting the custom-made set-up described above (Raman exciting wavelength = 266 nm). Synchrotron Raman spectrum recorded with an exciting wavelength of 226 nm (bottom) in the same conditions.

240 minutes), the peak is completely recovered (the discrepancy in the absorbance value is due to the dilution of the solution caused by the addition of oxidant and reductant solutions). After 240 minutes, the Raman spectrum (blue curves in Fig. 5) also shows the same vibrational mode of the pristine solution. The only difference is due to the rise of a broad contribution in the 1688–1620 cm^{-1} range, *i.e.* at frequencies quite different from that characterizing C=C stretching in cyclohexene (1651 cm^{-1}), thereby suggesting that new species are formed; unfortunately, resonance conditions obtained for CuBPA employing exciting light falling at 266 nm prevent the obtainment of much more clear signals. For this reason, the same reaction has been followed by adopting exciting light at 226 nm: the results are reported in the bottom panel of Fig. 5. It is worth noting here that under such conditions the broad signal is substituted by two narrower peaks centred at 1680 and 1620 cm^{-1} respectively, the highest one witnessing for the presence of a carbonylic species (*i.e.* C=O stretching) and the lowest for a conjugated C=C, probably the cyclohexanone that is one of the oxidation products of cyclohexene.[10,30,43] The presence of both cyclohexanone and cyclohexen-2-one (compatible with the vibration at 1620 cm^{-1}) has been further confirmed by GC-MS analyses (Fig. S18†). It should be noted that the MS spectrum of cyclohexanone is slightly more complicated than expected due to the dynamic equilibrium with cyclohex-1-en-1-ol (its enolic tautomer). We would like to stress that GC-MS spectra were collected as a control to justify the arising spectroscopic features. A more detailed analysis of the obtained products and the extension of the reaction scope will be discussed in a forthcoming paper.

Experimental

Materials and methods

All chemicals and solvents used were purchased from Merck (if not differently specified) and employed without further purification. 5,5′-Dimethyl-2,2′-bipyridine, 6,6′-dimethyl-2,2′-bipyridine and *tert*-butyl hydroperoxide were purchased from TCI. Copper complexes were synthesized under a N_2 atmosphere to prevent the oxidation of the metal centre and were obtained in excellent yield (>95%), according to a literature procedure. To oxidize the metal centre to Cu^{II}, hydrogen peroxide (30% in water), nitrosonium hexafluorophosphate and *tert*-butyl hydroperoxide (5.5 M in decane) were employed in appropriate ratios; cyclohexene was then used as an oxidizable substrate to verify the reversibility of the oxidation/oxygenation of the metal centre. A multi-technique approach was used to follow the redox cycle: cyclic voltammetry, Raman and UV-Vis-NIR.

Synthetic procedures

Synthesis of the ligand 6,6′-dimethoxy-2,2′-bipyridyl (BPC). The 6,6′-dimethoxy-2,2′-bipyridyl ligand was synthesized under a N_2 atmosphere to minimize the presence of water in the reaction mixture, according to a literature procedure.[26] A white solid was obtained with 80% yield (0340 g). ^{1}H NMR ($CDCl_3$): δ = 8.02 (2H, d), 7.68 (2H, dd), 6.75 (2H, d), 4.04 (6H, s).

General synthesis of copper(I) complexes. Copper complexes were synthesized following the literature reports[51] by mixing tetrakis(acetonitrile)copper(I) hexafluorophosphate and the bipyridine ligand (1 : 2 ratio) in anhydrous CH_2Cl_2. The solution was stirred under a N_2 atmosphere for three hours and, after stripping the solvent, the product was obtained as a coloured powder in excellent yield.

[Cu(6,6′-dimethyl-2,2′-bipyridyl)$_2$] (PF_6) (CuBPA). Following the above-mentioned general procedure, 0.98 g of the desired complex was obtained as a red powder with a yield of 98%. ^{1}H NMR (600 MHz, $(CD_3)_2CO$) δ 8.55 (d, J = 8 Hz, 1H), 8.20 (t, J = 8 Hz, 1H), 7.69 (d, J = 8 Hz, 1H), 2.35 (s, 3H), 2.09 (solvent residual peak).

[Cu(5,5′-dimethyl-2,2′-bipyridyl)$_2$] (PF_6) (CuBPB). Following the above-mentioned general procedure, 0.95 g of the desired complex was obtained as a violet powder with a yield of 95%. ^{1}H NMR (600 MHz, $(CD_3)_2CO$) δ 8.62 (d, J = 8 Hz, 1H), 8.58 (s, 1H), 8.13 (d, J = 8 Hz, 1H), 2.45 (s, 3H), 2.09 (solvent residual peak).

[Cu(6,6′-dimethoxy-2,2′-bipyridyl)$_2$] (PF_6) (CuBPC). Following the above-mentioned general procedure, 0.97 g of the desired complex was obtained as a dark powder with a yield of 97%. ^{1}H NMR (600 MHz, $(CD_3)_2CO$) δ 8.27 (m, 2H), 7.32 (d, J = 7 Hz, 1H), 3.76 (s, 3H), 2.09 (solvent residual peak).

[Cu(2,2′-bipyridyl)$_2$] (PF_6) (CuBPD). Following the above-mentioned general procedure, 0.97 g of the desired complex was obtained as a brown powder with a yield of 97%. ^{1}H NMR (600 MHz, $(CD_3)_2CO$) δ 8.81 (s, 1H), 8.35 (s, 1H), 7.82 (s, 1H), 2.09 (solvent residual peak).

NMR spectra details. The NMR spectra were recorded on a Jeol ECZ-R 600 MHz instrument, in $(CD_3)_2CO$, using the residual solvent peak as an internal reference ($(CD_3)_2CO$, ^{1}H: 2.09 ppm).[63] All the chemical shifts are reported in delta (δ) units. Coupling constants are reported in Hertz (Hz). Multiplicity is reported as follows: s (singlet), d (doublet), t (triplet), and m (multiplet). For each experiment, 8 scans were used with 5 s of relaxation and an acquisition time of 2.9 s. The spectra were recorded at −40 °C (Fig. S19–S22†).

Computational details. DFT simulations on Cu-complexes were performed with the Gaussian G16 (rev. B.01) code[64] by exploiting the hybrid B3LYP functional.[65] Unrestricted wavefunctions were adopted for all calculations, also when considering singlet states. Spin multiplicity was set to 1 (singlet state) for the initial Cu^I structures, whereas it was set to 2 (doublet) for Cu^{II} and hydro(pero)xo or 3 (triplet) for Cu^{II} oxyl models. The def2-TZVP basis set developed by Ahlrichs and coworkers[66] was adopted in the description of all atoms. Dispersive forces were included in the calculation through the Grimme D3 empirical scheme with Becke–Johnson damping.[67] The effect of solvation was implicitly accounted for *via* the polarizable conductor calculation model (CPCM) method.[68,69]

Fig. S3† shows the structure of the structural models adopted in the calculations of the starting Cu^I complexes. Their structure was manually constructed by positioning the

two bipyridyl ligands, oriented with the N atoms tetrahedrally coordinating the Cu atom at a distance of 2.0 Å. Counterion(s) were not included in the structural model. These initial models were geometrically optimized, and vibrational frequencies (including IR and Raman intensities) were computed. The absence of imaginary frequencies confirmed that minimum structures were obtained. From the optimized structures of the Cu^{I} complexes, Cu^{II} models were constructed by imposing the correct charge-spin, further optimized and adopted in frequency calculations. For the only CuBPA complex, we also simulated some hypothetical structures of Cu–O_x species, as expected to form upon interaction with *t*BuOOH, namely: Cu^{II}–$O(bpy)_2^+$ (oxyl), Cu^{II}–$OH(bpy)_2^+$ (hydroxo) and Cu^{II}–$OOH(bpy)_2^+$ (hydroperoxyl). Their optimized structures are shown in Fig. S13.† The main geometrical parameters for each model and their computed Cu^{I}/Cu^{II} oxidation potentials are reported in Tables S1 and S2.†

UV-Vis spectroscopic characterization. UV-Vis-NIR spectroscopy was performed on the samples with an Avantes AvaSpec-ULS2048XL-EVO fibre optics spectrometer (25 μm slits), coupled to an Avantes AvaLight-DH-S light source (equipped with a deuterium and a halogen lamp). Fibre optics with a high-OH fused silica core of 100 μm in diameter were used. Integration times and averaging were optimized for each sample to guarantee the best compromise between spectral and time resolution. The solutions were examined using Hellma flow-through high-performance quartz glass (QS grade) cuvettes with screw connections; depending on the concentration, a cuvette with an appropriate optical path length was selected between 0.1, 1 and 10 mm. The flow was regulated between the cuvette (s) and the liquid reservoir by means of a peristaltic pump using FEP (fluorinated ethylene propylene), PTFE (polytetrafluoroethylene) and fluorinated rubber connections.

Raman spectra of the solid powders of the Cu complexes. The whole set of Cu-based [2-2′-Bpy] homoleptic complexes in the form of solid powders were investigated through Raman Spectroscopy in order to obtain their major vibrational features. For the sake of comparison, all the parent [2-2′-Bpy] based ligands were also measured. Two different exciting laser lines (hereafter ELL) were adopted, emitting respectively at 785 nm (12 739 cm^{-1}) and 244 nm (40 984 cm^{-1}). Measurements were performed on a Renishaw Raman microscope equipped respectively with an Olympus 20× ULWD (NA = 0.40) and a Thorlabs UV-B 15× (NA = 0.31) objective through which the EEL was focused on the sample. The resulting back-scattered light (collected through the objectives described above) was then analysed respectively through 1200 l mm^{-1} and 3600 l mm^{-1} gratings. In order to prevent the possible thermal degradation of the investigated samples induced by the focused ELL, custom-made apparatus which allows holder movement (rotation) during measurements was adopted.[70] The presented spectra were obtained by averaging 3 consecutive measurements (from which the stability of the sample during the measurement was confirmed), each one resulting from the sum of 10 acquisitions of 20 s (ELL = 785 nm) or the sum of 20 acquisitions of 20 s each (ELL = 244 nm).

Raman spectra of the DCM solutions of the Cu complexes. Raman spectroscopy was adopted, as a complement to other techniques, to characterize, from a vibrational point of view, the whole set of Cu based [2,2′-bpy] homoleptic complexes (and, for the sake of comparison, their parent 2,2′-bpy based ligands) in the form of DCM solutions (a nominal concentration of 1 mM). Furthermore, a deep analysis of the obtained Raman spectra helped to get insights into the species formed when *tert*-butyl hydroperoxide was added in preparing the DCM solutions of such complexes. To overcome the possible drawbacks due to the low concentration, the 244 nm (40 984 cm^{-1}) ELL was adopted in order to exploit as much as possible the Resonant conditions. Measurements were performed on a Renishaw Raman Microscope equipped with a 15× (NA = 0.31) objective through which the ELL was focused on the sample. The resulting back-scattered light (collected through the objective) was then analysed by 3600 l mm^{-1} grating. Measurements were performed on the DCM solutions of the complexes placed in UV-Vis Hellma quartz (QS grade) cuvettes: the solutions were magnetically stirred continuously during the measurement thanks to the apparatus already described.[70] The presented spectra were obtained by averaging 3 consecutive measurements (from which the stability of the sample along the measurement was confirmed), each one resulting from the sum of 20 acquisitions of 20 s each.

Electrochemical characterization (cyclic voltammetry). Electrochemical characterization (cyclic voltammetry, CV) was performed by means of a BioLogic sp150 potentiostat. A three-electrode set-up was employed with a Pt disc (diameter = 5 mm) as the working electrode, a Pt wire as the counter-electrode and Ag/AgCl as the reference electrode. For the analysis of the Cu^{I} species, the complexes were dissolved (5 mM) in a solution of DCM containing tetrabutylammonium hexafluorophosphate ($TBAPF_6$, 0.1 M) as the supporting electrolyte. CVs were recorded at 100 mV s^{-1}. Before each measurement, the electrolyte was degassed with Argon to avoid the presence of oxygen. To analyse the oxidized sample, 0.1 ml of the *t*BuOOH solution was added to the Cu^{I} solution. A similar approach was employed when the effect of the cyclohexene as a reductant was investigated.

Raman spectra of the DCM solutions of the Cu complexes at the IUVS beamline. *In situ* Raman measurements on the systems described above were also performed by exploiting the facilities available at the BL10.2-IUVS beamline of Elettra Sincrotrone Trieste (Italy).[71] After the initial screening of some of the available exciting wavelengths, we resolved to use 266 nm (4.66 eV, 37 594 cm^{-1}) by regulating the undulator gap and using a Czerny-Turner monochromator (Acton SP2750, Princeton Instruments, Acton, MA, USA) equipped with a holographic grating at 1800 l mm^{-1} to monochromatize the incoming synchrotron radiation. Raman spectra were obtained in a back-scattered geometry by using a triple-stage spectrometer (Trivista, Princeton Instruments, Acton, MA, USA) with a spectral resolution of 2.3 cm^{-1} per pixel. Calibration of the spectrometer was standardized using cyclohexane. The possible photo/thermal damage effect due to the prolonged exposure of

the sample to exciting radiation was reduced by continuously moving the sample cell (UV-Vis Hellma quartz glass cuvette, QS grade) during the measurements. Each measurement consists of 30 scans of 30 seconds each, and then it is averaged between three successive scans.

UV-Vis/Raman simultaneous analyses at synchrotron. To provide simultaneous evidence on both the electronic transitions (UV-Vis-NIR) and vibrational modes (Raman, 266 or 226 nm exciting wavelength) of the selected complex undergoing a redox cycle, *i.e.* oxidation and reduction, a custom-made set-up was also employed (see Fig. S23†). This consists of a three-necked flask within which the investigated solution was allowed to recirculate thanks to a peristaltic pump. Two of the necks are closed with a PTFE stopper with two holes for the inlet and outlet tubes (1/16 inches diameter, in PTFE). The former goes from the flask (behaving as a reservoir) to the Raman (or UV-Vis-NIR) cuvette, whereas the latter makes the opposite. This system allows one to obtain a continuous flow of the solution. The reservoir is located halfway between the Raman and UV-Vis-NIR cuvettes to ensure the simultaneity between the two measurements. One should note that UV-Vis-NIR spectra were recorded each minute, whereas Raman spectra were recorded with a lower time resolution (each 15 minutes). The addition of the oxidant (and then of the reductant) was performed directly within the flask.

Gas chromatography/mass spectroscopy coupled analyses. GC-MS analyses were carried out on a trace Polaris q (by ThermoFischer), implemented with an Rxi 5Sil MS column (30 mm 0.25 mm 0.25um) with a Splitless injector using Helium (1 ml min^{-1}) as the gas carrier. The oven was initially set at 35 °C and the temperature was increased up to 150° C (ramp 10° C min^{-1}). The gas was detected by using an EI-Mass Spectrometer (T_{source} = 200 °C) working in the scan mode (m/z = 40–150) by means of an ionic trap analyser.

Conclusions

Throughout this paper, the redox behaviour of homoleptic copper 2,2′-bipyridine-based complexes toward the reaction with specific oxidants has been investigated by means of a multi-technique approach coupling electrochemistry and vibrational/electronic spectroscopy and supported by computational data. The selected complexes differ in the nature and the position of the substituent on the ligand skeleton. This has a dramatic influence on both the stability and the redox potential of the resulting complexes. Indeed, only CuBPA (*i.e.* [Cu(6,6′-dimethyl-2,2′-bipyridyl)$_2$] (PF_6) complex) exhibits a peculiar behaviour in the reaction with specific oxidants (*i.e.* *t*BuOOH or $NOPF_6$); indeed, the spectroscopic and electrochemical characterization of CuBPA gave some evidence of the formation of a (stable) Cu^{II} hydroxyl-species when reacted with *t*BuOOH, as proved by the appearance of an absorption peak at *ca.* 26 500 cm^{-1} (UV-Vis-NIR) and a marked shift of the peak located at 1014 cm^{-1} (Raman). By means of DFT calculations, this relatively stable oxygen-containing species was identified as Cu^{II}-OH$(bpy)_2^+$. These findings push us to further investigate the redox reactivity of CuBPA by means of a simultaneous UV-Vis-NIR/Raman experiment taking advantage of synchrotron facilities at Elettra: the formation of an oxygen-modified Cu^{II} species after the reaction with *t*BuOOH has been confirmed. Additionally, the latter could oxidize relatively fast a target compound (*i.e.* cyclohexene) and quantitatively form back the Cu^{I} complex, as also confirmed by electrochemical measurements. It should be noted that the specific reaction mechanism of the redox cycle is still under investigation taking advantage of both laboratories and synchrotron light-based experiments, but some oxygenated products have been already detected. The above-reported results open the way toward the application of Cu(BPA) as a precursor of a class of properly designed (homoleptic) copper bipyridine complexes in oxygenation reactions among which the Direct Methane to Methanol reaction is the most challenging one.

Author contributions

Conceptualization: C.B., M.B., and S.B. Data curation: B.C., G. D., A.D., M.S., and M.B. Formal analysis: B.C., G.D., A.D., M.S., and M.B. Funding acquisition: S.B. and C.B. Investigation: B. C., G.D., A.D., M.S., and M.B. Methodology: A.D., M.S., M.T., C.B., M.B., and S.B. Project administration: S.B. Resources: A. D., M.S., C.B., M.B. and S.B. Software: A.D. and M.S. Supervision: S.B., C.B., and M.B. Validation: B.C., G.D., A.D., M.S., and M.B. Visualization: B.C., G.D., A.D., and M.S., M.B. Writing - original draft: B.C., G.D., A.D., and M.B. Writing – review & editing: B.C., G.D., M.B., C.B., and S.B.

Conflicts of interest

The authors have no conflict of interest to declare.

Acknowledgements

The authors acknowledge the funding from Horizon 2020 Excellence Science ERC-Synergy program 2019-CUBE: "Unravelling the secrets of Cu-based catalysts for C–H activation" (grant agreement no. 856446). The authors acknowledge the CERIC–ERIC Consortium (project number 20207012, "Redox chemistry of model Cu complexes for direct alkane to alcohol conversion investigated by *in situ*/*operando* UV-Raman spectroscopy) for access to IUVS beamline facility at Elettra and financial support. The authors acknowledge the C3S consortium for granting computational resources on the OCCAM cluster, funded by the Compagnia di San Paolo. The authors thank the European Regional Development Fund and Interreg V-A Italy Austria 2014–2020 through the Interreg Italy-Austria project ITAT 1059 InCIMa4 "InCIMa for Science and SMEs". The authors are strongly indebted to Dr Alessandro Gessini and Dr Barbara Rossi (IUVS beamline staff) for technical support and to Dr Roberto Buscaino for the GC-MS measure-

ments. Dr Natale Porcaro is acknowledged for his help in the laboratory.

Notes and references

1 V. M. Goldschmidt, *J. Chem. Soc.*, 1937, 655–673.
2 Copper – Element information, properties and uses | Periodic Table, **https://www.rsc.org/periodic-table/element/29/copper**, (accessed 11 July 2021).
3 U.S. Geological Survay, **https://minerals.usgs.gov/minerals/**.
4 P. Nuss and M. J. Eckelman, *PLoS One*, 2014, **9**, e101298.
5 M. Soulier, S. Glöser-Chahoud, D. Goldmann and L. A. Tercero Espinoza, *Resour., Conserv. Recycl.*, 2018, **129**, 143–152.
6 R. Trammell, K. Rajabimoghadam and I. Garcia-Bosch, *Chem. Rev.*, 2019, **119**, 2954–3031.
7 C. E. Elwell, N. L. Gagnon, B. D. Neisen, D. Dhar, A. D. Spaeth, G. M. Yee and W. B. Tolman, *Chem. Rev.*, 2017, **117**, 2059–2107.
8 Y. S. Wei, M. Zhang, R. Zou and Q. Xu, *Chem. Rev.*, 2020, **120**, 12089–12174.
9 J. Baek, B. Rungtaweevoranit, X. Pei, M. Park, S. C. Fakra, Y. S. Liu, R. Matheu, S. A. Alshmimri, S. Alshehri, C. A. Trickett, G. A. Somorjai and O. M. Yaghi, *J. Am. Chem. Soc.*, 2018, **140**, 18208–18216.
10 X. Feng, Y. Song, J. S. Chen, Z. Xu, S. J. Dunn and W. Lin, *J. Am. Chem. Soc.*, 2021, **143**, 1107–1118.
11 L. Marais, H. C. M. Vosloo and A. J. Swarts, *Coord. Chem. Rev.*, 2021, **440**, 213958.
12 C. Kaes, A. Katz and M. W. Hosseini, *Chem. Rev.*, 2000, **100**, 3553–3590.
13 M. Magni, A. Colombo, C. Dragonetti and P. Mussini, *Electrochim. Acta*, 2014, **141**, 324–330.
14 D. B. Rorabacher, *Chem. Rev.*, 2004, **104**, 651–697.
15 S. Hattori, Y. Wada, S. Yanagida and S. Fukuzumi, *J. Am. Chem. Soc.*, 2005, **127**, 9648–9654.
16 C.-W. Lee and F. C. Ansen, *J. Phys. Chem.*, 1983, **87**, 3360–3362.
17 R. K. Kokal, S. Bhattacharya, L. S. Cardoso, P. B. Miranda, V. R. Soma, P. Chetti, D. Melepurath and S. S. K. Raavi, *Sol. Energy*, 2019, **188**, 913–923.
18 S. Maity, S. Kundu, T. Weyhermüller and P. Ghosh, *Inorg. Chem.*, 2015, **54**, 1300–1313.
19 L. Kavan, Y. Saygili, M. Freitag, S. M. Zakeeruddin, A. Hagfeldt and M. Grätzel, *Electrochim. Acta*, 2017, **227**, 194–202.
20 E. Tanaka, H. Michaels, M. Freitag and N. Robertson, *J. Mater. Chem. A*, 2020, **8**, 1279–1287.
21 A. Glinka, M. Gierszewski, B. Gierczyk, G. Burdziński, H. Michaels, M. Freitag and M. Ziółek, *J. Phys. Chem. C*, 2020, **124**, 2895–2906.
22 Y. Saygili, M. Stojanovic, H.-S. Kim, J. Teuscher, R. Scopelliti, M. Freitag, S. M. Zakeeruddin, J.-E. Moser, M. Grätzel and A. Hagfeldt, *J. Phys. Chem. C*, 2020, **124**, 7071–7081.
23 Y. Saygili, M. Söderberg, N. Pellet, F. Giordano, Y. Cao, A. B. Munoz-García, S. M. Zakeeruddin, N. Vlachopoulos, M. Pavone, G. Boschloo, L. Kavan, J. E. Moser, M. Grätzel, A. Hagfeldt and M. Freitag, *J. Am. Chem. Soc.*, 2016, **138**, 15087–15096.
24 C. Barolo, J. H. Yum, E. Artuso, N. Barbero, D. Dicenso, M. G. Lobello, S. Fantacci, F. Deangelis, M. Grätzel, M. K. Nazeeruddin and G. Viscardi, *ChemSusChem*, 2013, **6**, 2170–2180.
25 E. C. Constable, A. H. Redondo, C. E. Housecroft, M. Neuburger and S. Schaffner, *J. Chem. Soc., Dalton Trans.*, 2009, 6634–6644.
26 E. Fresta, G. Volpi, M. Milanesio, C. Garino, C. Barolo and R. D. Costa, *Inorg. Chem.*, 2018, **57**, 10469–10479.
27 M. D. Weber, C. Garino, G. Volpi, E. Casamassa, M. Milanesio, C. Barolo and R. D. Costa, *Dalton Trans.*, 2016, **45**, 8984–8993.
28 H. L. Kwong, W. S. Lee, H. F. Ng, W. H. Chiu and W. T. Wong, *J. Chem. Soc., Dalton Trans.*, 1998, 1043–1046.
29 X. Li, B. Zhang, R. Van Zeeland, L. Tang, Y. Pei, Z. Qi, T. W. Goh, L. M. Stanley and W. Huang, *Catal. Lett.*, 2018, **148**, 940–945.
30 J. M. Hoover and S. S. Stahl, *J. Am. Chem. Soc.*, 2011, **133**, 16901–16910.
31 J. E. Steves and S. S. Stahl, *J. Am. Chem. Soc.*, 2013, **135**, 15742–15745.
32 J. Kim and S. S. Stahl, *ACS Catal.*, 2013, **3**, 1652–1656.
33 X. Xie and S. S. Stahl, *J. Am. Chem. Soc.*, 2015, **137**, 3767–3770.
34 P. Gamez, I. W. C. E. Arends, J. Reedijk and R. A. Sheldon, *Chem. Commun.*, 2003, **3**, 2414–2415.
35 T. Sonobe, K. Oisaki and M. Kanai, *Chem. Sci.*, 2012, **3**, 3249–3255.
36 Y. F. Wang, H. Chen, X. Zhu and S. Chiba, *J. Am. Chem. Soc.*, 2012, **134**, 11980–11983.
37 T. Toyao, K. Miyahara, M. Fujiwaki, T. H. Kim, S. Dohshi, Y. Horiuchi and M. Matsuoka, *J. Phys. Chem. C*, 2015, **119**, 8131–8137.
38 D. Jiang, T. Mallat, D. M. Meier, A. Urakawa and A. Baiker, *J. Catal.*, 2010, **270**, 26–33.
39 B. Louis, C. Detoni, N. M. F. Carvalho, C. D. Duarte and O. A. C. Antunes, *Appl. Catal., A*, 2009, **360**, 218–225.
40 G. B. Shul'pin, Y. N. Kozlov and L. S. Shul'pina, *Catalysts*, 2019, **9**, 1046.
41 I. Garcia-Bosch and M. A. Siegler, *Angew. Chem., Int. Ed.*, 2016, **55**, 12873–12876.
42 K. Choroba, B. Machura, S. Kula, L. R. Raposo, A. R. Fernandes, R. Kruszynski, K. Erfurt, L. S. Shul'Pina, Y. N. Kozlov and G. B. Shul'Pin, *Dalton Trans.*, 2019, **48**, 12656–12673.
43 A. Sobkowiak, A. Qui, X. Liu, A. Llobet and D. T. Sawyer, *J. Am. Chem. Soc.*, 1993, **115**, 609–614.
44 H. Korpi, V. Sippola, I. Filpponen, J. Sipilä, O. Krause, M. Leskelä and T. Repo, *Appl. Catal., A*, 2006, **302**, 250–256.

45 B. Herzigkeit, B. M. Flöser, T. A. Engesser, C. Näther and F. Tuczek, *Eur. J. Inorg. Chem.*, 2018, **2018**, 3058–3069.
46 V. Leandri, Q. Daniel, H. Chen, L. Sun, J. M. Gardner and L. Kloo, *Inorg. Chem.*, 2018, **57**, 4556–4562.
47 F. Xu, T. Tao, K. Zhang, X. X. Wang, W. Huang and X. Z. You, *Dalton Trans.*, 2013, **42**, 3631–3645.
48 M. Munakata, S. Kitagawa and M. Miyazima, *Inorg. Chem.*, 1985, **24**, 1638–1643.
49 L. Palacios, A. Di Giuseppe, R. Castarlenas, F. J. Lahoz, J. J. Pérez-Torrente and L. A. Oro, *Dalton Trans.*, 2015, **44**, 5777–5789.
50 L. S. Shul'pina, M. M. Vinogradov, Y. N. Kozlov, Y. V. Nelyubina, N. S. Ikonnikov and G. B. Shul'pin, *Inorg. Chim. Acta*, 2020, **512**, 119889.
51 M. Giordano, G. Volpi, M. Bonomo, P. Mariani, C. Garino and G. Viscardi, *New J. Chem.*, 2021, **45**, 15303–15311.
52 L. Aronne, B. C. Dunn, J. R. Vyvyan, C. W. Souvignier, M. J. Mayer, T. A. Howard, C. A. Salhi, S. N. Goldie, L. A. Ochrymowycz and D. B. Rorabacher, *Inorg. Chem.*, 1995, **34**, 357–369.
53 M. Salavati-Niasari, P. Salemi and F. Davar, *J. Mol. Catal. A: Chem.*, 2005, **238**, 215–222.
54 C. J. Marzzacco, *J. Chem. Educ.*, 1999, **76**, 1517.
55 Y. Lu, D. Ng and M. S. Mannan, *Ind. Eng. Chem. Res.*, 2011, **50**, 1515–1522.
56 G. A. Mabbott, *J. Chem. Educ.*, 1983, **60**, 697.
57 F. Brunner, Y. M. Klein, S. Keller, C. D. Morris, A. Prescimone, E. C. Constable and C. E. Housecroft, *RSC Adv.*, 2015, **5**, 58694–58703.
58 N. Elgrishi, K. J. Rountree, B. D. McCarthy, E. S. Rountree, T. T. Eisenhart and J. L. Dempsey, *J. Chem. Educ.*, 2018, **95**, 197–206.
59 F. Roncaroli, M. Videla, L. D. Slep and J. A. Olabe, *Coord. Chem. Rev.*, 2007, **251**, 1903–1930.
60 C. M. Gallego, C. Gaviglio, Y. Ben-David, D. Milstein, F. Doctorovich and J. Pellegrino, *Dalton Trans.*, 2020, **49**, 7093–7108.
61 S. Keller, E. C. Constable, C. E. Housecroft, M. Neuburger, A. Prescimone, G. Longo, A. Pertegás, M. Sessolo and H. J. Bolink, *Dalton Trans.*, 2014, **43**, 16593–16596.
62 S. A. Bagshaw and R. P. Cooney, *J. Mater. Chem.*, 1994, **4**, 557–563.
63 H. E. Gottlieb, V. Kotlyar and A. Nudelman, *J. Org. Chem.*, 1997, **62**, 7512–7515.
64 M. J. Frisch, G. W. Trucks, H. B. Schlegel, G. E. Scuseria, M. A. Robb, J. R. Cheeseman, G. Scalmani, V. Barone, G. A. Petersson, H. Nakatsuji, X. Li, M. Caricato, A. V. Marenich, J. Bloino, B. G. Janesko, R. Gomperts, B. Mennucci, H. P. Hratchian, J. V. Ortiz, A. F. Izmaylov, J. L. Sonnenberg, D. Williams-Young, F. Ding, F. Lipparini, F. Egidi, J. Goings, B. Peng, A. Petrone, T. Henderson, D. Ranasinghe, V. G. Zakrzewski, J. Gao, N. Rega, G. Zheng, W. Liang, M. Hada, M. Ehara, K. Toyota, R. Fukuda, J. Hasegawa, M. Ishida, T. Nakajima, Y. Honda, O. Kitao, H. Nakai, T. Vreven, K. J. A. Throssell, Jr. Montgomery, J. E. Peralta, F. Ogliaro, M. J. Bearpark, J. J. Heyd, E. N. Brothers, K. N. Kudin, V. N. Staroverov, T. A. Keith, R. Kobayashi, J. Normand, K. Raghavachari, A. P. Rendell, J. C. Burant, S. S. Iyengar, J. Tomasi, M. Cossi, J. M. Millam, M. Klene, C. Adamo, R. Cammi, J. W. Ochterski, R. L. Martin, K. Morokuma, O. Farkas, J. B. Foresman and D. J. Fox, *Gaussian G16 (rev. B.01)*, 2016.
65 A. D. Becke, *J. Chem. Phys.*, 1993, **98**, 1372–1377.
66 F. Weigend and R. Ahlrichs, *Phys. Chem. Chem. Phys.*, 2005, **7**, 3297–3305.
67 S. Grimme, S. Ehrlich and L. Goerigk, *J. Comput. Chem.*, 2011, **32**, 1456–1465.
68 V. Barone and M. Cossi, *J. Phys. Chem. A*, 1998, **102**, 1995–2001.
69 M. Cossi, N. Rega, G. Scalmani and V. Barone, *J. Comput. Chem.*, 2003, **24**, 669–681.
70 M. Signorile, F. Bonino, A. Damin and S. Bordiga, *Top. Catal.*, 2018, **61**, 1491–1498.
71 B. Rossi, C. Bottari, S. Catalini, F. D'Amico, A. Gessini and C. Masciovecchio, in *Molecular and Laser Spectroscopy*, Elsevier, 2020, pp. 447–482.